ISSN: 0973-3469, Vol.21, No.(3) 2024, Pg. 115-133

Material Science Research India

www.materialsciencejournal.org

Punica Granatum – based Ternary Metal Oxide Nanoparticles: Degradation of Methylene Blue and Antimicrobial Study

MANITA THAKUR[1]*, ANKITA SHARMA[2], AJAY KUMAR[3], ARUSH SHARMA[4], SWATI KUMARI[5], AJAY SHARMA[6] and DEEPAK PATHANIA[7]

[1, 2, 6]Department of Chemistry, School of Basic and Applied Sciences, IEC University Baddi, Solan, India.
[3]Department of Chemistry, School of Basic and Applied Sciences, Maharaja Agrasen University, Himachal Pradesh, India.
[4]Department of Chemistry, School of Sciences, Baddi University of Emerging Sciences and Technology (BUEST), Himachal Pradesh, India.
[5]School of Biotechnology, Shoolini University of Biotechnology and Management Sciences, Solan, HP, India.
[7]Department of Environmental Science, Central University of Jammu, Bagla (Rahya-Suchani), Samba, Jammu and Kashmir, India.

Abstract

The production of nanoparticles derived from plant extracts has attracted considerable attention due to their cost-effectiveness, eco-friendly nature, and effective performance in different applications such as wastewater treatment and biomedicine. The present research emphasizes the eco-friendly synthesis of a nano-hybrid structure consisting of punica granatum (PGE) extract with zinc, lead, and manganese (ZPM). It is designed for efficient degradation of Methylene blue (MB) in nano-hybrid water systems. Punica granatum incorporated Zinc, lead and manganese (PGE/ZPM) nanohybrid structure was characterized using various techniques including FTIR (Fourier-transform infrared spectroscopy), FESEM (Scanning electron microscopy) with elemental mapping, HRTEM (Transmission electron microscopy), XPS (X-ray photoelectron spectroscopy) XRD (X-ray diffraction), TGA (Thermogravimetric analysis) and UV-Vis spectroscopy. The study included a thorough investigation of the optimization parameters specifically analyzing the effects of pH, dye concentration and catalyst dosage. The results showed that under solar exposure, 83.68% of Methylene blue (MB) was removed within 3 hours. The degradation mechanism follows

Article History
Received: 13 August 2024
Accepted: 22 November 2024

Keywords
Anti-Bacterial Activity;
Methylene Blue;
Photocatalysis;
Punica Granatum.

CONTACT Manita Thakur manitathakur1989@gmail.com Department of Chemistry, School of Basic and Applied Sciences, IEC University Baddi, Solan, India.

Doi: https://dx.doi.org/10.13005/msri/210303

pseudo-first order kinetics and the highest rate of degradation of MB at pH 6.0 was determined to be k= 0.0159 min-1. The photocatalyst was reused for five cycles, showing only a minor decline in degradation effectiveness. Antibacterial effectiveness of PGE, ZPM and PGE/ZPM was also assessed against *Staphylococcus aureus* (S. aureus) and *Escherichia coli* (E. coli). In summary, the cost-effective and environmentally friendly method used to synthesize PGE/ZPM has proven to be a versatile photo-catalytic and antibacterial agent.

Abbreviations

CB (Conduction band); (Initial concentration); Ct (Instant concentration at any time t of Methylene Blue); °C (Degree Celsius); electrons (e-); EDS Energy Dispersive X-Ray Spectroscopy; eV (Electron volt); *Escherichia coli* (*E. coli)*; FESEM (Scanning electron microscopy); FTIR (Fourier-transform infrared spectroscopy); Holes (h+); HRTEM (Transmission electron microscopy); JCPDS (Joint committee on powder diffraction strandards); k (rate constant); MB (Methylene Blue); min (Minute); nm (nanometer); pH (Potential of Hydrogen); % (percentage); PGE (*Punica granatum*); PGE/ZPM (*Punica granatum*- Zinc, lead and manganese); pzc (point of zero charge); *S. aureus Staphylococcus aureus*; SAED (Selected Area Electron Diffraction); UV-vis (Ultraviolet spectrophotometer); VB (Valence band); XRD (X-ray diffraction); XPS (X-ray photoelectron spectroscopy); Zinc, lead, and manganese (ZPM)

Introduction

One of the most significant issues facing human civilization throughout the world, especially in emerging countries is pollution.[1] All living things are seriously affected by the presence of contaminants in the water system. Polluted water is full of various toxic wastes such as heavy metals, dyes, micro-organisms, phenols, and pesticides etc.[2] Pollution is the discharge of toxic substances into the atmosphere that harm people or other living things and pollute the environment. These pollutants may appear as chemical substances or as energy in the form of noise, heat and light.[3] It has a negative impact on environmental resources like clean air and water supplies. Pollution has detrimental effects on canals, glaciers, oceans, reservoirs, and aquifers, causing them to become polluted. It occurs when harmful toxic waste or contaminated materials are dumped directly into the water bodies. The increasing discharge of domestic, industrial and agricultural waste effluents into the water system poses significant issues for the developing world. The entire fauna and flora were seriously threatened by organic pollutants such as phenols, dyes, fertilizers, toxic metals and pesticides.

Industrial pollution is the release of waste and pollutants produced by human activities into the environment including air, water and land. This can degrade ecosystems, kill animals, destroy vegetation and have negative effects on human health. Pollution affects both biodiversity of living organisms and individuals in their daily lives. Industrial pollutants released into water bodies cause significant biological and chemical oxygen demands disturbing the natural balance by reducing aquatic biodiversity and the photosynthetic activity of aquatic life.[4] The pollution of the marine system because of many industrial activities has become a matter of serious concern.[5] Cadmium, copper, aluminum, chromium, thorium, and cobalt are examples of toxic metals that cause disease in living organisms. Several techniques such as ion exchange, adsorption, photocatalysis, filter-based separation and chemical precipitation formation have been employed to remove toxic substances from the environment.[6] Research and development on the atomic, molecular or macromolecular scale referred to as nanotechnology. Particles with at least one dimension of 100 nm are considered nanoparticles, which are the fundamental units of nanotechnology. The environmental quality of air, water, and soil can be greatly improved via nanotechnology. This may facilitate the development of new cleaning technologies which enhance the detection and sensing of contaminants.[7] For the production of green nanoparticles, metals have been intensively used because of their use in biomedicine and industries. Silver has gained a great deal of interest for its ability to produce plant-based green silver nanoparticles. When reduced with organic materials

like plant extracts, and various incredibly essential elements like Copper, Zinc Oxide, Iron, lead nitrate, manganese chloride and gold nanoparticles form highly beneficial green nanoparticles.[8] The main focus has recently been placed on the production of food-grade nanoparticles from natural components such as lipids, proteins and carbohydrates.[9] The removal of organic pollutants and noxious microbes using sunlight has been suggested as a potential application of nanoparticles. The efficiency of photocatalysts is assessed through light absorption, which excites electrons (e^-) from the valence band (VB) to the conduction band (CB), creating a hole (h^+) in the VB and triggering photo redox processes instantaneously.[10] In semiconductors, the band gap energy is the amount of energy required to excite an electron from the valence band to the conduction band. Predicting photophysical and photochemical properties of semiconductors requires accurate calculations of the band gap energy.[11]

The presence of dyes in effluents poses a significant problem due to their harmful effects on living organisms. The discharge of dyes into the environment is a source of concern for both toxicological and visual effects.[12] Methylene blue (MB) is a cationic dye commonly utilized for dying cotton, wool and silk. The presence of this color in dirty water can cause a burning sensation in the eyes, nausea, vomiting and many diseases. The visible region of 660nm exhibits the highest absorption of methylene blue.[13] The molecular structure of MB is shown in Scheme 1.

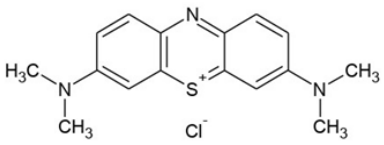

Scheme 1: Molecular structure of Methylene blue

Anaar (Punica-granatum) is often referred as pomegranate and is a member of the Lythraceae family with the confirmed species being *Punica granatum provence*. The words pomegranate meaning “full of seeds” and pomum which means “apple” are both derived from Latin. It is a beautiful shrub and has orange- red flowers in the spring season. In the Middle East, India and China Punica-granatum has been used for future generations in long-established medicine to cure a variety of illnesses from pain and irritation. The best-known use is as a vermifugal or taenicidal agent which kills and expels intestinal worms.[14] Fruit residues are the subject of intense investigation because they are rich in diverse phenolic chemicals, which could be beneficial in prevention and treatment of a variety of ailments including cancer, diabetes and cardiovascular illness. It is well known that the peel of pomegranate contains a number of phenolics with significant biological potential, including penduncalin, punicalagin, ellagic acid and gallic acid.[15] On the other hand, Pomegranate is extensively used in industrial waste which has wide nutritional value. In recent years, pomegranates have been used as antioxidant, antibacterial and antifungal properties to treat many diseases. Pomegranate is also used to eliminate organic pollutants due to its photocatalytic activity.[16] It is one of the earliest eatable fruits and is commonly grown in various tropical and sub-tropical nations has been documented in various research. Pomegranate is one of the foods that can prevent diseases like atherosclerosis and brain dysfunction.[17] Organic compounds found in plant extracts can undergo redox reactions and also serve to stabilize and cap synthesized agents. The outer coat extract of *Punica granatum* is known to act as reducing co-surface capping agent associated with the synthesis of nanoparticles. Capping agents are important as stabilization agents that prevent the nanoparticles from growing too much and clumping together during colloidal synthesis.[18]

Metal nanoparticles can be classified as monometallic, bimetallic, or tri-metallic depending on the presence of metal or metal oxides. Transition bi- and tri-metallic nanoparticles have greater catalytic selectivity/ activity and better efficiency in many applications than monometallic nanoparticles, and they can also function as heterogeneous nano-reactants in variety of organic processes.[19] A developing field, particularly focused on trimetallic nanoparticles in catalysis was motivated by the advantages of adding other metals to nanoparticle catalysts such as palladium, zinc, lead, manganese and gold nanoparticles.[20]

This study aims to synthesize composite with powder of outer coat of *Punica granatum* (pomegranate) and a tri-metal composite comprising zinc, lead and manganese (ZPM) via co-precipitation method.

The PGE/ZPM composite is then tested for its effectiveness as a photocatalyst in the degradation of Methylene blue (MB) under various conditions. Additionally, its anti-bacterial properties are evaluated against two common microbial strains, *Staphylococcus aureus* (*S. aureus*) and *Escherichia coli* (*E. coli)*.[21]

Materials and Methods

In this preparation, Zinc chloride, lead nitrate, manganese chloride, and sodium hydroxide were purchased from CDH Pvt. Ltd. All the solutions were prepared in de-ionized water. Punica-granatum fruit was referred to Lythraceae family and obtained from Baddi, Himachal Pradesh.

Preparation of *Punica-Granatum* (Pg) Outercoat Extract

Punica granatum, commonly known as pomegranate or anar, fruits were collected and washed thoroughly under running water After washing, the outer coat of the pomegranate was removed and dried for a week. Once fully dried, the outer coat was crushed into fine powder.[22]

Synthesis of *Punica-granatum*- Zn/Pb/Mn (PGE/ZPM) Nanoparticles

In this method, 0.1 Molar Zinc chloride, 0.1 Molar Lead nitrate, 0.1 Molar Manganese chloride was prepared in a 1:2:1 ratio in a 500 mL beaker with continuous stirring. After that, add a few drops of NaOH solution to maintain basic pH. Further, finely powdered Punica-granatum outer coat extract was added in fixed quantity to the above solution. The above mixture was stirred for two hrs. at 60°C and then allowed to cool. The solution was filtered and rinsed twice to thrice times with double-distilled water to remove impurities. In this way, different samples were prepared, and the best one was used for further studies.[23]

Characterization Techniques

The morphologies of nanoparticles were characterized by high-resolution transmission electron microscopy (HR-TEM) using a FP 5022/22-Tecnai G2 20 S-Twin TEM instrument. Field emission scanning electron microscopy (FESEM) with elemental mapping performed by Nova Nano SEM 450, FEI Tecnai instrument. The X-ray diffraction (XRD) patterns of the synthesized nanoparticles were collected by using Rigaku 9 kW rotating anode x-ray diffractometer with Cu Kα radiation. The surface compositions of the synthesized nanoparticles were analyzed by X-ray photoelectron spectroscopy (XPS) using PHI 5000 Versa Probe spectrometer. Fourier Transform Infra-Red (FTIR) spectrum of synthesized nanoparticles was noted by Perkin–Elmer, USA, model Spectrum-BXSHIMADZU 1730 (range of 4000–400 cm^{-1}).

Photocatalytic Activity

The efficiency of photocatalytic degradation of PGE/ZPM nanoparticles was evaluated for the removal of methylene blue (MB). For this, a solution of MB was prepared at fixed concentration and a definite amount of PGE/ZPM was added into the MB solution. Then, solution was exposed to solar light and 3-5 mL of liquid sample withdrawn after fixed intervals of time and absorbance was recorded in UV spectrophotometer at λmax. In this way, different values of absorbance were recorded at different time and percent degradation value was calculated by formula given below.[24]

$$\% \text{ Degradation} = (C_o - C_t)/C_o$$

Where, = C_o initial concentration

C_t = instant concentration at any time t of MB

The degradation kinetics were analysed using pseudo- first order reaction model and rate constant (K) was determined using equation as mentioned:

$$K = 2.303 \times \text{slope}$$

Where, slope was determined from the graph of ln (absorbance) versus t.

Antimicrobial activity

The antimicrobial activity of PGE/ZPM nanoparticles was evaluated using the well diffusion method against both gram-negative and gram-positive bacterial isolates, including *Staphylococcus aureus* and *Escherichia coli*. Bacteria were cultured on nutrient agar media for this assay. A lawn culture of the isolates was prepared on nutrient agar plates, and wells were created using a puncture tool. Each well received 100 µl (100 mg/ml) of PGE/ZPM, while ampicillin (10 mg/ml) served as positive control, and triple-distilled autoclaved water was used as a negative control. The plates were incubated at 37°C

for 16-18 hours to allow bacterial growth. All tests were conducted in triplicate. Inhibition zones around the wells were measured using a Hi Media antibiotic zone scale, and the diameters of these zones were recorded in milimeters (mm).[25]

Results and Discussion

Synthesis of Punica-granatum Zn/Pb/Mn (PGE/ZPM) nanoparticles by co-precipitation method. In the first step, the addition of Zinc chloride, Lead nitrate and manganese chloride in a fixed ratio to prepare trimetallic nanoparticles (ZPM). When organic part was added to ZPM a new material was formed with improved structure, morphology and properties. PGE bioactive compounds attach to the nanoparticle surfaces, introducing functional groups (e.g. hydroxyl, carbonyl, carboxyl) which improve reactivity, biocompatibility and surface properties. The organic molecules from the PGE outer coat stabilize the nanoparticles by forming a protective layer, preventing agglomeration and enhancing particle dispersity. Green synthesis of PGE/ZPM nanoparticles was performed by varying percentage of organic part as described in Table 1. Sample S-3 was studied in detail as it shows better results as compared to other S-0, S-1, S-2, S-4 and S-5.

Table 1: Optimized preparation conditions for PGE/ZPM nanoparticles

S.No.	Zinc Chloride (0.1M)	Lead Nitrate (0.1M)	Manganese Chloride (0.1M)	*Punica-granatum* outercoat powder (%)	Color	Temp.
S-0	1	2	1	-		
S-1	1	2	1	0.4	yellow	50-60°C
S-2	1	2	1	0.8	Light yellow	50-60°C
S-3	1	2	1	1.2	Pale yellow	50-60°C
S-4	1	2	1	1.6	Light yellow	50-60°C
S-5	1	2	1	2.0	Light yellow	50-60°C

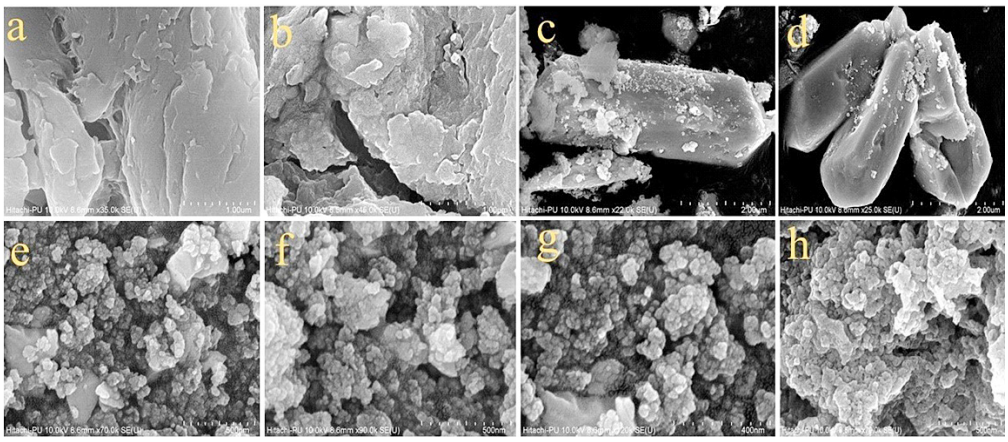

Fig. 1: a: FESEM images at various magnifications :(a & b) PGE, (c & d) ZPM, (e-h) PGE/ZPM, (i) EDS elemental mapping surface of PGE/ZPM, and (j-n) images of elemental mapping PGE/ZPM

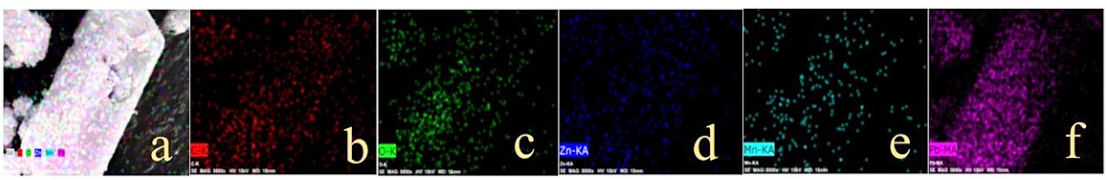

Fig. 1 b: FESEM (a-f) images of elemental mapping of PGE/ZPM

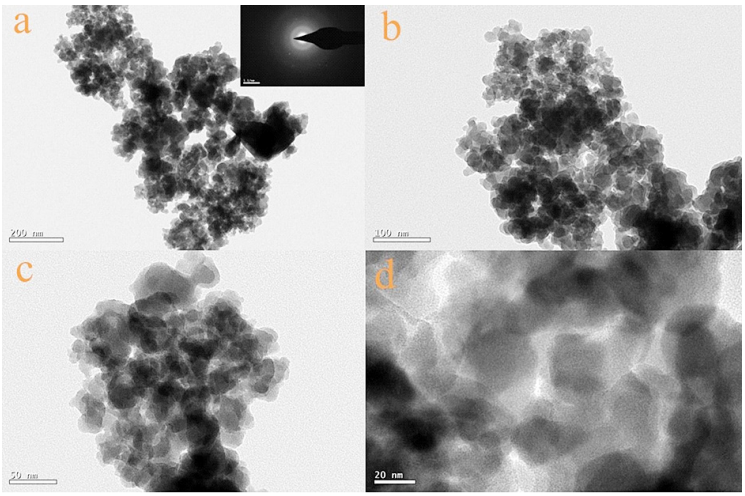

Fig. 2: (a-d) TEM images of (PGE/ZPM) (inset SAED pattern)

Characterization

FESEM and HRTEM

Fig. 1. a: (a, b) reveals that *Punica granatum* extract (PGE) particles exhibit varied sizes and shapes, featuring rough edges and significant microfractures on their surfaces.[26] Fig. 1: (c, d) of inorganic part show octahedral crystals with indications of blister formation and surface roughening. However, no complete fracture or separation of fragments is evident in these figures.[27] Fig. 1: (e - h) shows the presence of organic material in the sample, evidenced by clumped sizes of the nanoparticles.[28,29] The aggregation of small particles may be the reason for the existence of some larger particles. The addition of any impurity in pure substance causes a substantial change in the particle morphology.[30] The homogenous distribution of materials in the PGE/ZPM nanoparticles is demonstrated through EDS mapping of the elements shown in Fig. 1. b: (a - f).[31] The HRTEM images of synthesized PGE/ZPM nanoparticles at various magnifications are shown in Fig. 2: (a - d). PGE/ZPM consists of layer-shaped nanoparticle clusters that include spherical and cubic-shaped nanoparticles.[32] The average particle size of PGE/ZPM was calculated to be 23.06 nm which correlates with the data obtained from XRD. This confirms the presence of PGE/ZPM in nanoparticle form.[33] SAED pattern implies that the prepared samples have crystalline properties.[34]

XRD Study

The diffraction pattern exhibits a broad peak centered around 2 theta at 20°, indicates the amorphous nature of PGE as shown in Fig. 3: (a). This peak arises from the presence of bioactive molecules like polyphenols, flavonoids and tannins which lack a crystalline structure. In Fig. 3: (b) the diffraction peaks at 2 theta value of lead at 24°, 30°, and 40° are shown with JCPDS no. 005- 0592 indexed as (210) (200), (220).[35] The diffraction peaks at 2 theta values of 29°, and 35° of Mn are indexed with JCPDS no. 77-0471 at (112), and (211) at 18°, 51° with JCPDS no. 41-1442.36 The diffraction peaks of Zn at 27°, 43°, 47° are indexed with JCPDS no. 36-1451 at (200), (102) at 25°, 56° indexed with (101), (110) which shows sharp narrow peaks and good crystallinity of the nanoparticles.[37,38] The XRD pattern of the PGE/ZPM retains the sharp peaks associated with the crystalline ZPM nanoparticles confirming complete cojugation of PGE in Fig. 3: (c). The sharp peaks of PGE/ZPM at 18°, 24°, 25°, 27°, 30°, 33°, 35°, 39°, 43°, 47°, 51° and 56°. The diffraction peaks observed at 2 theta 24°, 30° and 40° correspond to the (210), (200), (220) are indicative of PbO with JCPDS card no. 38-1477. The presence of PbO suggests the successful precipitation of lead ions into their oxide form.[39] The diffraction peaks observed at 2 theta values of 33°, and 35°, correspond to (112) and (211) planes of MnO, MnO_2 with JCPDS card no. 44-0141 at 18°, 51° with planes of (111), (440) Mn2O3, JCPDS card No. #01-07-1826. The prominent peaks observed at 27°, 47°, 56° correspond to (200), (102), (110) planes of ZnO JCPDS card no. 36-1451 respectively, at 25°, 43° indexed as (101), (101) with JCPDS card no 65-9226. These peaks confirm the formation of

ZnO.[40] The peaks in the PGE/ZPM pattern appear slightly broader compared to ZPM. This broadening may result from reduced crystallite size or incresed strain introduced by the interaction between the bioactive compounds from PGE/ZPM nanoparticles. The peak intensities in the PGE/ZPM nanoparticle are noticeably lower comapred to the ZPM. In PGE/ZPM the corresponding peaks are present but with reduced intensity, indicating the retention of crystallinity with some reduction caused by PGE.[41] According to De bye Scherrer formula, the average grain size of the nanoparticles was around 23.06 nm in Fig. 3: (c). And it was calculated by this formula.[42]

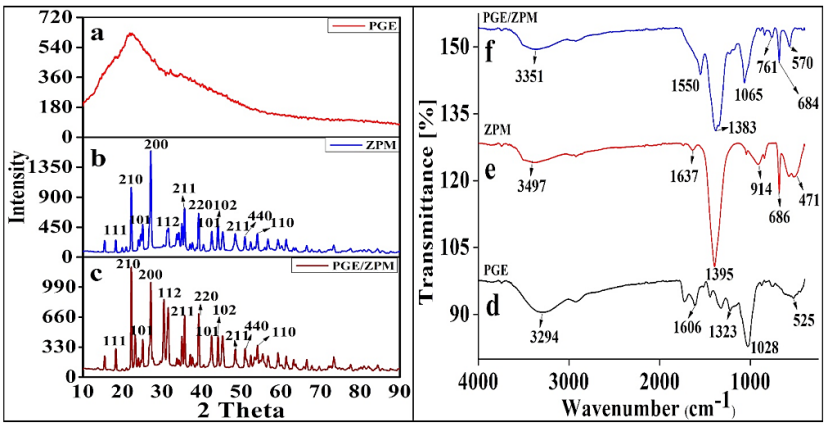

Fig. 3: XRD and FTIR graph of (a) (d) PGE, (b) (e) ZPM, and (c) (f) PGE/ZPM

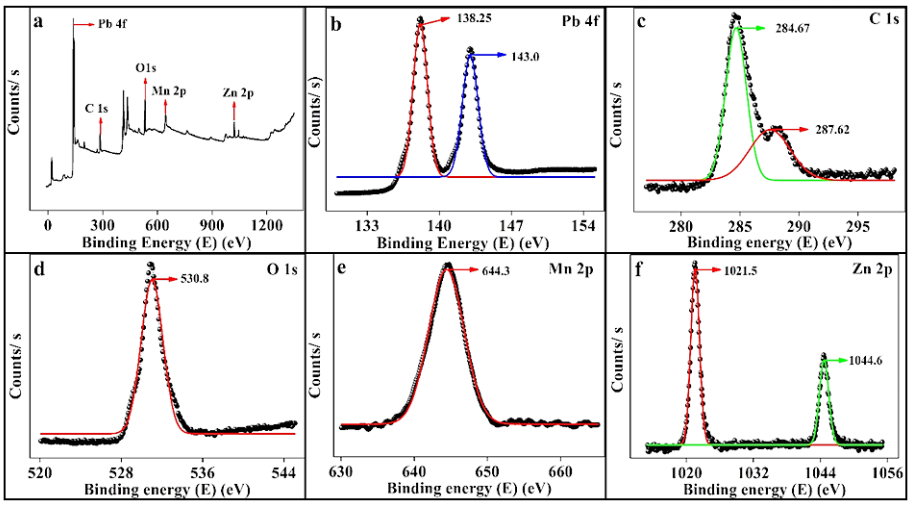

Fig. 4: XPS survey graph of (a) Survey, (b) Pb, (c) C, (d) O, (e) Mn, and (f) Zn

$$B = K \lambda \mid \cos \theta \quad ...(3)$$

FTIR Study

Fig. 3: (d) shows individual FTIR spectrum of PGE. At 3294 cm^{-1} broad peak corresponds to OH vibrations.43 The peak at 1606 cm^{-1} is due to aromatic carbon.44 At 1323 cm^{-1} due to primary and secondary aromatic amines.[45] A broad peak at 1028 cm^{-1} refers to C-O-C symmetric and asymmetric vibrations.[46] At 525 cm^{-1} corresponds to C-C stretching vibration.[47] Fig. 3: (e) shows FTIR spectrum of ZPM at 3497 cm^{-1} peak refers to OH vibrations.[48] The sharp peak at 1395 cm^{-1} was due to C=O stretching vibrations.[49] The medium peak at 1637 cm^{-1} represented the C-C=C symmetric stretching of conjugated alkene groups.[50] The peak at 914 cm^{-1} refers to C-H out plane vibration.[51] The peak at 686 cm^{-1} and 471 cm^{-1} are due to metal

oxides. Fig. 3: (f) illustrates the FTIR spectra of PGE/ZPM at 3351 cm^{-1} peak refers to OH vibrations. The new peak at 1550 cm^{-1} is due to -CO and COO- symmetric and asymmetric vibrations.[52] The peak at 1383 cm^{-1} is due to the addition of PGE into ZPM refers to C-H bending vibrations. The peak at 1065 cm^{-1} was due to C-O and C-N symmetric stretching of aliphatic amines.[53] The peaks at 570 cm^{-1}, 684 cm^{-1} and 761 cm^{-1} are due to metal oxides Mn-O, Pb-O, and Zn-O.[54]

XPS Study

Fig. 4: (a) displays the results of XPS analysis of the chemical structure of PGE/ZPM. The elements C, O, Mn, Zn and Pb are found in nano-hybrid. In Fig. 4: (b) The maximal energy peak at 138.25 ev and 143 ev which relate to Pb 4f 7/2 for PbO and Pb 4f 5/2 for PbO_2.[55] In Fig. 4: (c) the maximal binding energy peak measured at 287.62 and 284.67 ev is attributed to C-C and π – π* bonding of the C1s, which is due to the presence of C-C/ C-H bond.[56] Fig. 4: (d) the maximal binding energy peak measured at 530ev of O1s may be attributed to lattice oxygen in lattice crystal due to free hydroxyl group.[57] In Fig. 4: (e) Mn shows the oxidation state for Mn 2p 3/2 peak at 644 indicate the presence of multiple oxidation states for Mn in the respective sample.[58] Fig. 4: (f) the binding energy peaks of Zn 2p 3/2 at 1022 ev for ZnO and Zn 2p ½ for ZnO_4 were measured at 1044 ev.[59]

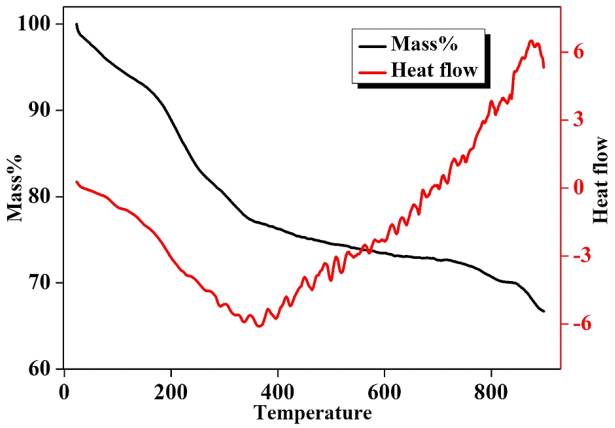

Fig. 5: TGA and DSC graph of PGE/ZPM

TGA

In Fig. 5: Thermogravimetric analysis (TGA) was used to analyze the thermal characteristics and gas evolution of the materials. The samples were placed within an alumina crucible and heated using N_2 flow at a rate of 10°C per minute.[60] Due to evaporation of water, it turns out that there is a gradual 6% weight loss before 150°C. There is more significant drop in mass between 150°C to 350°C indicating 20% loss most likely as a result of thermal degradation of the organic material in the sample, destabilization of the organic compounds and dehydration.[61] The final degradation occurring from 350°C to 800°C with 7% weight loss is attributed to decomposition of polymer.[62] The wide thermal adsorption peak between 300 and 400°C in the DSC profile was due to solid-phase components as precipitates. A zig-zag pattern may indicate multiple phase transitions. The material undergoes crystallization and then melts or undergoes multiple polymorphic transitions. A stable endothermic (heat absorption) behavior is observed at the beginning of the curve at 0°C to 200°C. A slight zigzag in this area may result in loss of volatile substances or minor physical changes. The mid-temperature range from 200°C to 400°C indicates more noticeable zigzag patterns which suggest that multiple thermal events have occurred.[63] A specific thermal process, such as the breakdown of various components inside the sample is represented by each peak. It is suggested that endothermic peaks include evaporation of bound water and breaking of chemical bonds. The highest temperature range at 400°C to 800°C signifies the result of last stages of component decomposition or melting.[64] The upward trend towards the end indicates ongoing endothermic processes. It indicates that these components undergo significant thermal changes within the temperature range. This process involves

the absorption of heat and significant structural changes in the material leading to a semi-crystalline state over a broad temperature range.[65]

Optical Studies

Using the tauc relation, the band gap of ZPM, PGE/ZPM nanoparticles was determined i.e. Eg = 3.29 and 2.54 eV respectively. The results showed that, when it comes to light in the UV-Vis region, the PGE/ZPM nanoparticles exhibit competitively higher efficiency than ZPM. The tauc plot, is presented in Fig. 6: (a, b).[66]

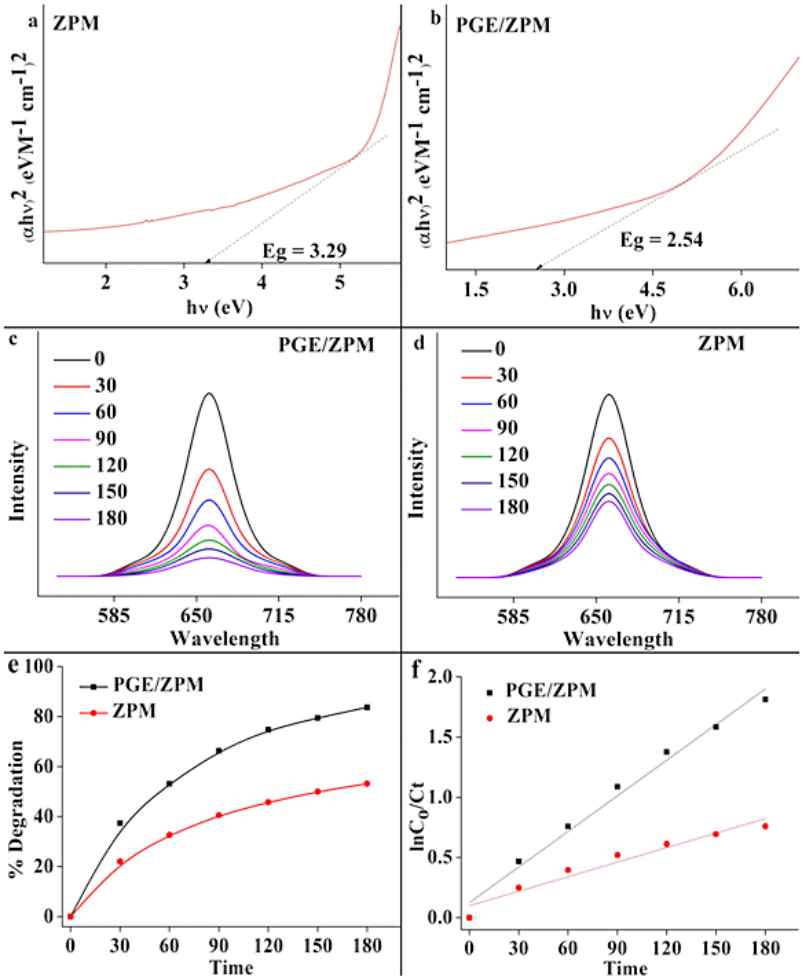

Fig. 6: Tauc plots for (a) ZPM, (b) PGE/ZPM, Ultraviolet spectrum of (c) PGE/ZPM, (d) ZPM with MB, (e) % deterioration of PGE/ZPM and ZPM over time, and (f) pseudo-first-order kinetic plot for the deterioration of MB

Photodegradation

The photodegradation activity of PGE/ZPM and ZPM was determined by investigating the degradation of Methylene blue under natural visible light irradiation. The surface of the photocatalyst undergoes photochemical generation of holes and electrons when exposed to light radiation. Photogenerated electrons moving from the valence band (VB) to the conduction band create a positively charged hole (H^+) in the VB of the photocatalyst.[67] By exciting electrons to higher energy levels, the photocatalyst minimizes the recombination of photogenerated holes (h^+) and electrons (e^-). On the surface of the photocatalyst surface, oxidation and reduction processes occur whereby excited electrons reduce molecular oxygen to the superoxide radical O_2 or free radical. A hole

generated from electron excitation transforms the hydroxyl ion into an OH-free radical. The primary active species, holes and electrons undertake redox reactions to produce secondary active species, free radicals and harmless free radicals from O_2 and water/OH ions.[67] This degradation pathw8y is shown in Scheme 2. The possible mechanism of photodegradation can be explained on the basis of:

PGE/ZPM + Light energy → PGE/ZPM ($^{e-}$cb + $^{h+}$vb)
PGE/ZPM ($h^{+}{}_{vb}$) + H2O → PGE/ZPM + H+ $OH^{\cdot}$
PGE/ZPM ($h^{+}{}_{vb}$) + OH → PGE/ZPM + $OH^{\cdot}$
PGE/ZPM ($^{e-cb}$) + O_2 → PGE/ZPM + $O^{\cdot}{}_2$
$O^{\cdot}{}_2$ + H+ $HO^{\cdot}{}_2$
$HO^{\cdot}{}_2$ + $O^{\cdot}{}_2$ → $OH^{\cdot}$ + OH^{-} + O_2
H_2O_2 + $O^{\cdot}{}_2$ → $OH^{\cdot}$ + OH^{-} + O_2
MB + OH → Degradation process

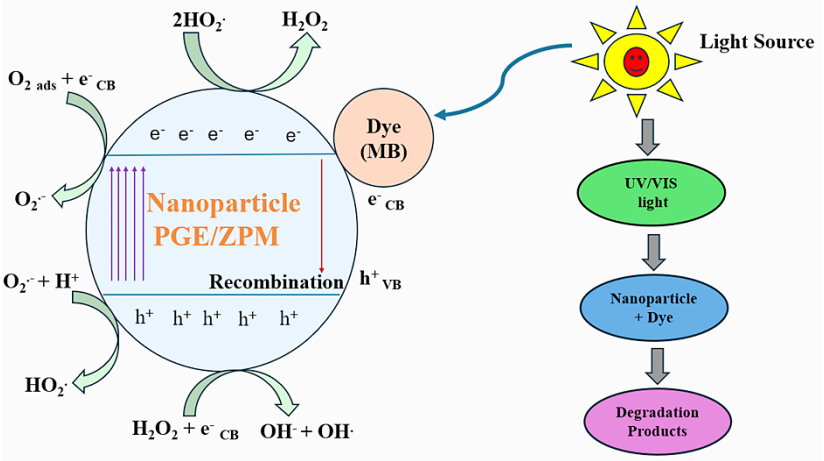

Scheme 2: Photocatalytic degradation pathway of MB

Fig. 6: (c, d) shows the UV spectra of MB at various time intervals of light exposure, both with PGE/ZPM and ZPM. The gradual reduction in peak intensity indicates a decrease in the concentration of MB.

Fig. 6: (e) displays the percentage photodegradation degradation of MB as a function of time in the presence of PGE/ZPM and ZPM. After 180 minutes under the sun radiation, it was found that 83.68% of MB gets degraded. The degradation efficiency of PGE/ZPM is as follows: PGE/ZPM (83.68%) > ZPM (53.15%). Fig. 6: (f) shows the photodegradation process which follows pseudo- first order kinetics and their values shown in Table 2. Compared with its photocatalyst counterpart, the rate constant for PGE/ZPM was determined to be 0.0099 min^{-1} which was a higher value.

Table 2: Rate and half–life period values of photodegradation reaction of Methylene Blue

Toxin	**Methylene Blue**	
Sample	**Rate (min-1)**	**Half-life period (min)**
PGE/ZPM	0.0099	30.395
ZPM	0.0092	75.22

Electrostatic attraction between the surfaces of dye and catalyst can be used to explain the effect of pH variation. The electrostatic interaction is dependent on two factors: the pKa value of the MB and point of zero charge of PGE/ZPM. 3.8 is the Pka value of MB.69 When the pH value fluctuates from the pKa constant value, the dye molecule exhibits both cationic and anionic forms. For the catalyst, the point zero charge (Pzc) is determined to be 7.5 as illustrated in Fig. 7. As the pH value increases and

decreases the catalyst surface gains and loses charge. Influence of pH on the removal of MB in the presence of PGE/ZPM and ZPM in the pH range of 2.0-12.0. MB is a cationic dye that demonstrates the impact of pH on PGE/ZPM adsorption. According to the Pzc assay, the PGE/ZPM dye degradation rate reached its peak at pH of 6 (k= 0.0159). At pH 6, the highest amount of MB was removed. When the dye dissolves in water the positively charged ions are released. Therefore, in an acidic media the positively charged surface of the sorbents prevents cationic adsorption. The opposing charges on the surfaces of MB and PGE/ZPM at pH 6 cause more interactions between the molecules thereby increasing the rate of MB.[70] The photodegradation percentage of MB at various pH values using PGE/ZPM and ZPM is shown in Fig. 8: (a, b).

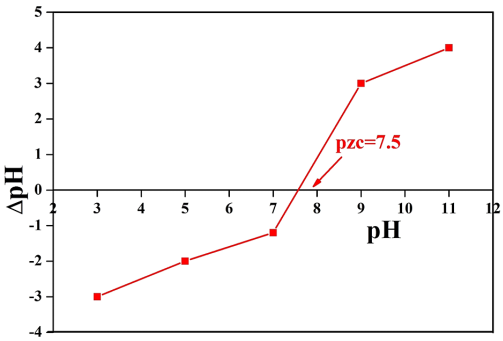

Fig. 7: Point of zero charge (pzc) of PGE/ZPM

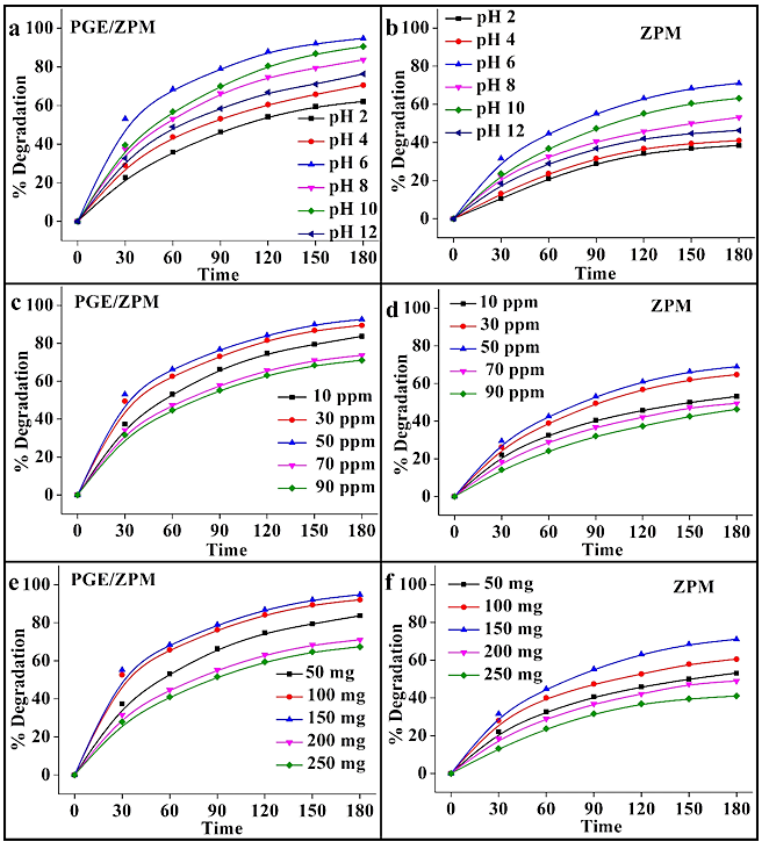

Fig. 8: Effect of pH on % degradation of (a) PGE/ZPM, (b) ZPM with MB, The influence of MB concentration on the percentage degradation with (c) PGE/ZPM, (d) ZPM, and The impact of catalyst on the percentage degradation of MB using (e) PGE/ZPM, (f) ZPM

The impact of MB concentration was examined within the range of 10-90 ppm. Fig. 8: (c, d) shows the rate values for PGE/ZPM and PGE at different dye concentrations. The rate of removal of MB was maximum 0.0320 min^{-1} with PGE/ZPM and 0.0141 min^{-1} ZPM for 50 ppm of MB concentration. Rate falls as MB concentration increases and depletion of active sites with high concentrations of MB is the

reason for the degradation. The photodegradation process is interrupted when all active sites are saturated.[71]

The impact of photo-catalyst dosage was examined within the range of 50 to 250 mg. Fig. 8: (e, f). illustrates the impact of catalyst loading on the percentage of MB degradation when using PGE/ZPM. The maximum rate of MB degradation was 0.0361 min^{-1} with 150 mg for PGE/ZPM and for ZPM was 0.0156 min^{-1} (Table 3). When the dosage exceeds 150 mg, the rate begins to decline because high concentrations of catalysts form turbidity which slows the rate at which sunlight interacts with pollutants.[72]

Table 3: Effect of parameters on the degradation of Methylene Blue

Methylene Blue									
		pH			Dye concentration			Catalyst dose	
		Rate (min^{-1})	Half-life period (min)		Rate (min^{-1})	Half-life period (min)		Rate (min^{-1}) (min)	Half-life period
PGE/ZPM	2	0.0124	55.724	10 ppm	0.0228	30.395	50 mg	0.0028	30.395
ZPM		0.0064	107.46		0.0092	75.227		0.0092	75.227
PGE/ZPM	4	0.0149	46.294	30 ppm	0.0278	24.868	100 mg	0.0313	22.125
ZPM		0.0069	100.30		0.0131	52.791		0.0112	61.410
PGE/ZPM	6	0.0227	30.395	50 ppm	0.0320	21.648	150 mg	0.0361	19.166
ZPM		0.0092	75.227		0.0141	47.017		0.0156	44.252
PGE/ZPM	8	0.0366	18.925	70 ppm	0.0165	41.793	200 mg	0.0156	44.251
ZPM		0.0156	44.251		0.0085	81.327		0.0085	81.327
PGE/ZPM	10	0.2993	23.147	90 ppm	0.0156	44.251	250 mg	0.0140	49.329
ZPM		0.0126	54.711		0.0078	88.503		0.0069	100.30
PGE/ZPM	12	0.0177	39.079						
ZPM		0.0078	88.503						

Antibacterial Activity

The result of antibacterial activity of PGE/ZPM nanoparticles against gram positive bacteria: *Staphylococcus aureus*; gram negative bacteria: *Escherichia coli* was recorded. PGE/ZPM and antibiotic (ampicillin) demonstrated effective inhibition zones against various pathogens, as illustrated in Fig. 9: (a, b). The inhibition zones, measured in milimeters and listed in Table 4 were observed against *Escherichia coli* and *Staphylococcus aureus*. These zones were measured around PGE/ZPM and ampicillin in different wells.[25]

Table 4: Zones of inhibition produced by nanoparticles against diverse pathogenic strains

Bacteria	Ana1	Ana2	Ana3	Positive control	Negative control
Escherichia coli	19±0.58	16±0.42	10±0.51	24±0.56	ND
Staphylococcus aureus	20.5±0.46	8±0.50	17.8±0.55	22±0.49	ND

Reusability and Stability

The stability and reusability of the fabricated photocatalyst are important components of practical application. Fig. 10: (a) shows the results of a 5-cycle test conducted on the reusability of PGE/ZPM. The obtained data indicate that PGE/ZPM-NPs exhibit exceptional stability after five cycles of MB degradation, with a slight loss in their catalytic

activity. This may be attributed to the inability of the photocatalyst to completely degrade MB due to blocking of some active sites.[73] Fig. 10: (b) depicts the FTIR spectra of PGE/ZPM after the fifth cycle of reusability. The high stability of the nanoparticles was confirmed by the absence of any significant peak shifts.[74] Fig. 10: (c) shows the FTIR spectra of PGE/ZPM and Methylene blue loaded PGE/ZPM.[75] The peak values and intensities of Methylene Blue on nanoparticle surfaces are altered by photocatalytic degradation.[76] FTIR spectrum of MB nanoparticles indicates a new peak at 3650 cm^{-1} due to CO ion and hydroxyl groups. The new peak at 3540 cm^{-1} due to stretching vibrations of free hydroxyl indicating the formation of hydrogen bonds during adsorption.[77] The signal shifted from 2915 cm^{-1} to 2924 cm^{-1} due to stretching vibration of -CH_2 group.[78] Peak at 1383 cm11 due to vibration of C=S and C-N bond moved to 1395 cm^{-1}.[79] Peak at 1550 cm^{-1} due to vibration of aromatic ring and C-N bond shifted to 1558 cm^{-1}.[80] The signal shifted from 1065 cm^{-1} to 1071 cm^{-1} due to stretching vibrations of primary amines.[81] Peak at 680 cm^{-1} due to waving vibration of C-N.[82] This was proven to be the reason for the breakdown of MB molecules in the presence of the nanocomposite and their adsorption on the PGE/ZPM molecular assembly from the aqueous solution, thereby reducing the concentration of polluting dye in the aqueous solution.[83]

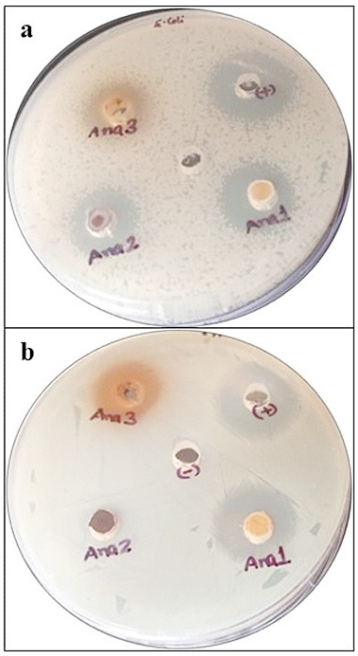

Fig. 9: Antimicrobial analysis of nanoparticles against various pathogenic bacteria (a) showed antimicrobial activity against *E. coli*, (b) showed antimicrobial activity against *Staphylococcus aureus*, "+" represents Positive control, "-" represents Negative control. Ana1 represents PGE/ZPM, Ana 2 represents ZPM, Ana 3 represents PGE

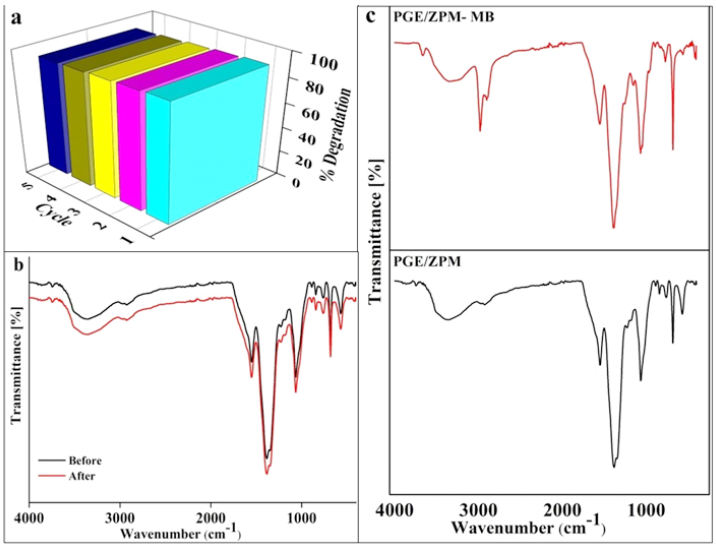

Fig. 10: Effect of pH on % degradation of (a) PGE/ZPM, (b) ZPM with MB, The influence of MB concentration on the percentage degradation with (c) PGE/ZPM, (d) ZPM, and The impact of catalyst on the percentage degradation of MB using (e) PGE/ZPM, (f) ZPM

Conclusion

Nano-hybrid structures consisting of Zn/Pb/Mn trimetallic nanoparticles incorporated with punica-granatum extract were fabricated using Co-precipitation method. Nanoparticles were characterized by different spectral techniques like FTIR, FESEM, HRTEM, XRD, XPS and TGA. Methylene blue (MB) was effectively removed by PGE/ZPM when exposed to radiance. The photocatalytic reaction rate was examined by using pseudo- first order kinetics which showed that, after 3 hours of solar exposure 83.68% of MB was degraded. The antibacterial activity of PGE/ZPM against *S. aureus* and E. coli bacteria was evaluated. Therefore, PGE/ZPM nanoparticles exhibits high efficiency in the treatment of pollutants. The fabrication of trimetallic inorganic moieties represents a novel approach in nanomaterial synthesis which offers vast potential for further exploration and study.

Acknowledgement

The authors would like to thank Panjab University (PU) and the Indian Institute of Technology (IIT) Mandi, providing the necessary equipment facilities to conduct the present research.

Funding Sources

The author(s) received no financial support for the research, authorship, and/or publication of this article.

Conflict of Interest

The authors declare that none of the work described in this paper is influenced by any known competing financial interests or personal relationships.

Data Availability Statement

The manuscript incorporates all datasets produced or examined throughout this research study.

Ethics Statement

This research did not involve human participants, animal subjects, or any material that requires ethical approval.

Informed Consent Statement

This research did not involve human participants, and therefore, informed consent was not required.

Clinical Trial Registration

This research does not involve any clinical trials

Author Contributions

- **Dr. Manita Thakur:** have performed software, supervision, investigation, writing original draft, writing.
- **Dr. Ajay Kumar and Dr. Arush Sharma:** performed the writing—original draft, validation, visualization, writing.
- **Ms. Ankita Sharma:** has done conceptualization, data curation, methodology and software work.
- **Ajay Sharma and Dr. Swati Kumari:** carry out the formal analysis, administration and resources.
- **Dr. Deepak Pathania:** overall review & editing.

References

1. Al Naggar. Y, Khalil M. S and Ghorab M. A. Environmental pollution by heavy metals in the aquatic ecosystems of Egypt. *J. Toxicol.,* 2018; 3: 555603.
2. Pathania D, Agarwal S, Gupta V. K, Thakur M and Alharbi N. S. Zirconium (IV) phosphate/poly (gelatin-cl-alginate) nanocomposite as ion exchanger and Al3+ potentiometric sensor. *Int. J. Electrochem. Sci*., 2018; 13: 994-1012.
3. Duruibe J. O, Ogwuegbu M. O and Egwurugwu J. N. Heavy metal pollution and human biotoxic effects. *Int. J. Phys. Sci.,* 2007; 2:112-8.
4. Kaur K and Jindal R. Synergistic effect of organic-inorganic hybrid nanocomposite ion exchanger on photocatalytic degradation of Rhodamine-B dye and heavy metal ion removal from industrial effluents. *Environ Chem Eng.,* 2018; 6: 7091-101.

5. Pathania D, Thakur M, Sharma G and Mishra A. K. Tin (IV) phosphate/poly (gelatin-cl-alginate) nanocomposite: Photocatalysis and fabrication of potentiometric sensor forPb (II). *Mater. Today Commun.,* 2018; 14: 282-93.
6. Thakur M, Pathania D, Sharma G, Naushad M, Bhatnagar A and Khan M. R. Synthesis, characterization and environmental applications of a new bio-composite gelatin-Zr (IV) phosphate. . *Environ. Polym. Degrad*., 2018; 26: 1415-24.
7. Biswas P and Wu C. Y. Nanoparticles and the environment. *J. Air Waste Manag. Assoc.,* 2005; 55 :708-46.
8. Khan T, Ullah N, Khan M. A and Nadhman A. Plant-based gold nanoparticles; a comprehensive review of the decade-long research on synthesis, mechanistic aspects and diverse applications. *Adv. Colloid Interface Sci.,* 2019; 272: 102017 .
9. Chen X, Chen Y. Zou, Zhang X, Dong Y, Tang J, McClements D. J and Liu W. Plant-based nanoparticles prepared from proteins and phospholipids consisting of a core–multilayer-shell structure: Fabrication, stability, and foamability. *J. Agric. Food Chem.,* 2019; 67: 6574-84.
10. Mills A and Le Hunte S. An overview of semiconductor photocatalysis. *J. Photochem. Photobiol.,* A., 1997; 108 :1-35.
11. Makuła P, Pacia M and Macyk W. How to correctly determine the band gap energy of modified semiconductor photocatalysts based on UV–Vis spectra. *J. Phys. Chem. Lett.,* 2018; 9: 6814-7.
12. Rafatullah M, Sulaiman O, Hashim R and Ahmad A. Adsorption of methylene blue on low-cost adsorbents: a review. *J. Hazard. Mater.,* 2010; 177: 70-80.
13. Salehi M, Hashemipour H and Mirzaee M. Experimental study of influencing factors and kinetics in catalytic removal of methylene blue with TiO_2 nanopowder. *Am J Environ Engineer*., 2012; 2: 1-7.
14. Arun N, and Singh D. P. *Punica granatum*: a review on pharmacological and therapeutic properties. *IJPSR*. 2012; 3: 1240-5.
15. Santos M. P, Souza M. C, Sumere B. R, da Silva L. C, Cunha D. T, Bezerra R. M and Rostagno M. A. Extraction of bioactive compounds from pomegranate peel (*Punica granatum* L.) with pressurized liquids assisted by ultrasound combined with an expansion gas. *Ultrasonics sonochemistry.,* 2019; 54: 11-7.
16. Al-Zahrani S. A, Patil M. B, Mathad S. N, Patil A. Y, Otaibi A. A, Masood N, Mansour D, Khan A, Manikandan A and Syafri E. Photocatalytic degradation of textile orange 16 reactive dye by ZnO nanoparticles synthesized via green route using *Punica granatum* leaf extract. *Cryst.*, 2023; 13: 172.
17. Tehranifar A, Selahvarzi Y, Kharrazi M and Bakhsh VJ. High potential of agro-industrial by-products of pomegranate (*Punica granatum* L.) as the powerful antifungal and antioxidant substances. *IND CROP PROD.,* 2011; 34:1523-7.
18. Nazar N, Bibi I, Kamal S, Iqbal M, Nouren S, Jilani K, Umair M and Ata S. Cu nanoparticles synthesis using biological molecule of P. granatum seeds extract as reducing and capping agent: Growth mechanism and photo-catalytic activity. *Int. J. Biol. Macromol.,* 2018; 106: 1203-10.
19. Nasrollahzadeh M, Sajjadi M, Iravani S and Varma R. S. Trimetallic nanoparticles: greener synthesis and their applications. *Nanomater.,* 2020; 10: 1784.
20. Crawley J. W, Gow I. E, Lawes N, Kowalec I, Kabalan L, Catlow CR, Logsdail A. J, Taylor S. H, Dummer N. F and Hutchings G. J. Heterogeneous trimetallic nanoparticles as catalysts. *Chem. Rev.,* 2022;122 :6795-849.
21. Kumari A, Kumar A, Thakur M, Pathania D, Rani A and Sharma A. Murraya Koenigii Plant-Derived Biochar (BC) and Lanthanum Ferrite ($BC/LaFeO_3$) Nano-Hybrid Structure for Efficient Ciprofloxacin Adsorption from Waste Water. *Chem. Afr.,* 2023; 16: 1-7.
22. Alwash A. The green synthesize of zinc oxide catalyst using pomegranate peels extract for the photocatalytic degradation of methylene blue dye. *Baghdad Sci. J.,* 2020; 17 :0787.
23. Kondalkar M, Fegade U, Attarde S and Ingle S. Experimental investigation on phosphate adsorption, mechanism and desorption properties of Mn-Zn-Ti oxide trimetal alloy nanocomposite. *JDS&T*. 2018; 39:1635-43.
24. Pathania D, Thakur M, Sharma A, Agarwal S and Gupta V. K. Synthesis of lactic acid–Zr (IV) phosphate nanocomposite ion

exchanger for green remediation. *Ionics.*, 2017; 23: 699-706.

25. Sharma A, Thakur M, Kumar A, Gautam M, Kumari S, Pathania D and Sharma A. Efficient photodegradation of fast sulphon black and crystal violet dyes from water systems using locust bean gum (LBG)-encapsulated zirconium-based nanoparticles and antibacterial activity. *Nanotechnol. Environ. Eng.*, 2023; 8: 859-77.
26. Pathak P. D, Mandavgane S. A and Kulkarni B. D. Characterizing fruit and vegetable peels as bioadsorbents. *Curr. Sci.*, 2016; 10: 2114-23.
27. Tong F, Al-Haidar M, Zhu L, Al-Kaysi R. O and Bardeen C. J. Photoinduced peeling of molecular crystals. *Chem. Commun.,* 2019; 55: 3709-12.
28. Ahmad H, Venugopal K, Rajagopal K, De Britto S, Nandini B, Pushpalatha H. G, Konappa N, Udayashankar A. C, Geetha N and Jogaiah S. Green synthesis and characterization of zinc oxide nanoparticles using Eucalyptus globules and their fungicidal ability against pathogenic fungi of apple orchards. *Biomol.* 2020;10: 425.
29. Cao Y, Du S, Chen T. T, Chen M, and Wang H. J. Effects of inorganic antiseptic on the properties of zein-based active films. *J. Environ. Polym. Degrad.,* 2018; 26: 4430-40.
30. Silambarasan M, Saravanan S and Soga T. Mn-doped ZnO nanoparticles prepared by solution combustion method. *E-j. surf. sci. nanotechnol.,* 2014; 12: 283-8.
31. Kumar A, Chandel M, Sharma A, Thakur M, Kumar A, Pathania D and Singh L. Robust visible light active PANI/LaFeO3/CoFe2O4 ternary heterojunction for the photo-degradation and mineralization of pharmaceutical effluent: Clozapine. *Environ. Chem. Eng.*, 2021; 9: 106159.
32. Duraimurugan J, Kumar GS, Maadeswaran P, Shanavas S, Anbarasan P. M and Vasudevan V. Structural, optical and photocatlytic properties of zinc oxide nanoparticles obtained by simple plant extract mediated synthesis. *J. Mater. Sci.: Mater. Electron.*, 2019; 30: 1927-35.
33. Adarakatti P. S, Gangaiah V. K, Banks C. E and Siddaramanna A. One-pot synthesis of Mn 3 O 4/graphitic carbon nanoparticles for simultaneous nanomolar detection of Pb (II), Cd (II) and Hg (II). *J. Mater. Sci.*, 2018; 53: 4961-73.
34. Gigot A, Fontana M, Pirri C. F and Rivolo P. Graphene/ruthenium active species aerogel as electrode for supercapacitor applications. *Mater.,* 2017; 11: 57.
35. Adeyemi J. O and Onwudiwe D. C. Nanoparticles Prepared Using 1, 10-Phenanthroline Adduct of Lead (II) Bis (N-alkyl-N-phenyl dithiocarbamate) as Single Source Precursors. *Mol.* 2020; 25: 2097.
36. Chen L, Zhang Q, Yao J, Wang J, Kong W, Jiang C and Chang A. Formation of Mn-Co-Ni-O nanoceramic microspheres using in situ ink-jet printing: sintering process effect on the microstructure and electrical properties. *Small,* 2016; 12: 5027-33.
37. Azam A and Babkair SS. Low-temperature growth of well-aligned zinc oxide nanorod arrays on silicon substrate and their photocatalytic application. *Int. J. Nanomedicine., 2*014; 9: 2109.
38. Adeyemi J. O and Onwudiwe D. C. PbS Nanoparticles Prepared Using 1, 10-Phenanthroline Adduct of Lead (II) Bis (N-alkyl-N-phenyl dithiocarbamate) as Single *Source Precursors. Mol.,* 2020; 25: 2097.
39. Behzad S. K, Najafi E, Amini M. M, Tadjarodi A, Dehghani A and Notash B. Synthesis, characterization, and optical properties of lead (II) coordination polymers and nanosize lead oxide core of polymer. *Monatsh. Chem.,* 2015; 146: 35-45.
40. Ali A. T and Karem L. K. Biosynthesis, Characterization, Adsorption and Antimicrobial studies of Manganese oxide Nanoparticles Using *Punica granatum* Extract. *Baghdad Sci. J.* 2024; 21: 0952.
41. Krishnapriya K. R and Kandaswamy M. A new chitosan biopolymer derivative as metal-complexing agent: synthesis, characterization, and metal (II) ion adsorption studies. *Carbohydr. Res.,* 2010; 345: 2013-22.
42. Muniz F. T, Miranda M. R, Morilla dos Santos C and Sasaki J. M. The Scherrer equation and the dynamical theory of X-ray diffraction. *Acta Crystallogr A Found Adv.,* 2016; 72 :385-90.
43. Prakash O, Selvi M. K, Vijayaraj P and Kudachikar V. B. nutraceuticals and nutritional

profiling of Pyrus pashia Buch.-ham ex D. Don (Kainth) seeds oil and its antioxidant potential. F*ood Chem.*, 2021; 338: 128067.

44. Li Z, Fredericks P. M, Ward C. R and Rintoul L. Chemical functionalities of high and low sulfur Australian coals: A case study using micro attenuated total reflectance–Fourier transform infrared (ATR–FTIR) spectrometry. *Org. Geochem.,* 2010; 41: 554-8.
45. Carballo T, Gil M. V, Gómez X, González-Andrés F and Morán A. Characterization of different compost extracts using Fourier-transform infrared spectroscopy (FTIR) and thermal analysis. *Biodegradation.,* 2008; 19: 815-30.
46. Popescu V, Sandu I. C and Popescu G. FTIR analysis for studying the possibility of grafting onto cotton of some compounds resulted from the interaction of carbonyl compounds with monochlorotriazinyl-β-cyclodextrin. *Rev. Chim.*, 2016; 67: 2184-9.
47. Mopoung S, Singse W and Sirikulkajorn A. Preparation of metal-carbon composites from banana peel charcoal and metal salts for hydrogen storage by pyrolysis method. *J Indian Chem Soc*., 2014 ;91: 1071-8.
48. Xie X. Z, Kuang H, Weins E, Deevsalar R, Tunc A, Purdy S, Zuin L, Tse J. S, Mi J. X and Pan Y. Synthesis of jadarite in the Li 2 O–Na 2 O–B 2 O 3–SiO 2–NaCl–H 2 O system: FTIR, Raman, and Li and BK-edge XANES characterizations and theoretical calculations. *EJM.,.* 2024; 36 :139-51.
49. Sakthivel P, Muthukumaran S and Ashokkumar M. Structural, band gap and photoluminescence behaviour of Mn-doped ZnS quantum dots annealed under Ar atmosphere. *J. Mater. Sci.: Mater. Electron.,* 2015; 1533-42.
50. Suganya K, Hari R and Chokkalinagam P. Synthesis of zinc oxide nanoparticles using stem extract of Citrullus colocynthis, characterization and evaluation of its antibacterial activity. *nat. remedies.,* 2023; 23: 1101-1106.
51. Nasser A, Migahed M. A, Basiony N. M, Abd-El-Bary H. M and Mohammed T. A. Raman and Infrared Spectral Analysis, Normal Coordinate Analysis, DFT calculations of Novel Schiff Base Containing di-imine moieties. *Egypt. J. Chem.,* 2023; 66: 271-91.
52. Salokhe A, Koli A, Jadhav V, Mane-Gavade S, Supale A, Dhabbe R, Yu X. Y and Sabale S. Magneto-structural and induction heating properties of MFe_2O_4 (M= Co, Mn, Zn) MNPs for magnetic particle hyperthermia application. *SN Appl. Sci.* 2020 ;2: 2017.
53. Ifeanyichukwu U. L, Fayemi O. E and Ateba C. N. Green synthesis of zinc oxide nanoparticles from pomegranate (*Punica granatum*) extracts and characterization of their antibacterial activity. *Mol.,* 2020; 25: 4521.
54. Sheikh Z, Amin M, Khan N, Khan M. N, Sami S. K, Khan S. B, Hafeez I, Khan S. A, Bakhsh E. M and Cheng CK. Potential application of Allium Cepa seeds as a novel biosorbent for efficient biosorption of heavy metals ions from aqueous solution. *Chemosphere.*, 2021; 279: 130545.
55. Yi N, Wang S, Duan Z, Wang K, Song Q and Xiao S. Tailoring the Performances of Lead Halide Perovskite Devices with Electron-Beam Irradiation. *Adv. Mater.,* 2017; 29 :1701636.
56. Ameen S, Akhtar M. S, Kim Y. S and Shin H. S. Nanocomposites of poly (1-naphthylamine)/SiO2 and poly (1-naphthylamine)/TiO2: Comparative photocatalytic activity evaluation towards methylene blue dye. *Appl. Catal., B.,* 2011; 103:136-42.
57. Biswas P. K, De A, Dua L. K and Chkoda L. Surface characterization of sol-gel derived indium tin oxide films on glass. *Bull. Mater. Sci.*, 2006; 29: 323-30.
58. Nagaraju G, Sekhar S. C, Ramulu B, Hussain S. K, Narsimulu D and Yu J. S. Ternary MOF-based redox active sites enabled 3D-on-2D nanoarchitectured battery-type electrodes for high-energy-density supercapatteries. *Nanomicro Lett.*, 2021;13:1-8.
59. Bankar D. B, Hawaldar R. R, Arbuj S. S, Moulavi M. H, Shinde S. T, Takle S. P, Shinde M. D, Amalnerkar D. P and Kanade KG. ZnCl 2 loaded TiO 2 nanomaterial: An efficient green catalyst to one-pot solvent-free synthesis of propargylamines. *RSC Adv.,* 2019; 9 :32735-43.
60. Barbosa S. L, Nelson D. L, Paconio L, Pedro M, Dos Santos W. T, Wentz A. P, Pessosa F. L, Agbleyor F. A, Bortoleto D. A, Fretias-Marques M. B and Zanatta L.

D. Environmentally friendly new catalyst using waste alkaline solution from aluminum production for the synthesis of biodiesel in aqueous medium. *Bioeng.,*2023; 10 :692.

61. Huang Y, Lin Y. C, Jenkins D. M, Chernova N. A, Chung Y, Radhakrishnan B, Chu I. H, Fang J, Wang Q, Omenya F and Ong S. P. Thermal stability and reactivity of cathode materials for Li-ion batteries. *ACS Appl. Mater. Interfaces:*., 2016; 8: 7013-21.
62. Mahto A and Mishra S. Guar gum grafted itaconic acid: a solution for different waste water treatment. *Environ. Polym. Degrad.,* 2021; 1: 1-4.
63. El Moujahed S, Errachidi F, Abou Oualid H, Botezatu-Dediu A. V, Chahdi F. O, Rodi Y. K and Dinica R. M. Extraction of insoluble fibrous collagen for characterization and crosslinking with phenolic compounds from pomegranate byproducts for leather tanning applications. *RSC Adv.,* 2022; 12 :4175-86.
64. Khan S. A, Mohd Zain Z, Siddiqui Z, Khan W, Aabid A, Baig M and Abdul Malik M. . Development of Magnesium Aluminate (MgAl2O4) Nanoparticles for refractory crucible application. *Plos one.,* 2024; 19: 0296793.
65. Villacrez J. L, Carriazo J. G and Osorio C. Microencapsulation of Andes Berry (*Rubus glaucus Benth.*) aqueous extract by spray drying. *FABT.* 2014; 7: 1445-56.
66. Akhtar M, Bibi I, Majid F, Ghafoor A, Kamal S, Fatima Q, Raza N, Alwadai, A and Nazir M. Iqbal. Photoluminescence, structural, optical, ferroelectric and photo-catalytic properties of magnetically separable CdO/$CoFe_2O_4$ hetero-junction. *Ceram. Int.*, 2024; 50: 13573-13581.
67. Paz C. V, Fereidooni M, Hamd W, Daher E. A, Praserthdam P and raserthdam S. Analysis of Ag-DP25/PET plasmonic nano-composites as a visible-light photocatalyst for wastewater treatment: Experimental/theoretical studies, and the DFT-MB degradation mechanism. *Environ. Res.,* 2024; 252: 119081.
68. Lanjwani M. F, Tuzen M, Khuhawar M. Y and Saleh T. A. Trends in photocatalytic degradation of organic dye pollutants using nanoparticles: a reviewInorg. *Chem. Commun*., 2024; 159: 111613.
69. Sousa H. R, Silva L. S, Sousa P. A, Sousa R. R, Fonseca M. G, Osajima J. A and Silva-Filho E. C. Silva-Filho, Evaluation of methylene blue removal by plasma activated palygorskites. *JMR&T.* 2019; 8 :5432-42.
70. Azeez F, Al-Hetlani E, Arafa M, Abdelmonem Y, Nazeer A. A, Amin M. O and Madkour M. The effect of surface charge on photocatalytic degradation of methylene blue dye using chargeable titania nanoparticles. *Sci. Rep.* 2018; 8: 1-9.
71. Amil M, Akhtar M. N, Imran M, Javaid A, Zafar H. K, Sohail M, ALDamen M. A, Fitta M, Khanfar M. A, and Al-Qawasmeh R. A. Photocatalytic degradation of methylene blue dye and electrocatalytic water oxidation over copper (II) complex with mixed ligands. *JPPA* .2024; 446: 115095.
72. Siong V. L, Lee K. M, Juan J. C, Lai C. W, Tai X. H and Khe C. S. Removal of methylene blue dye by solvothermally reduced graphene oxide: a metal-free adsorption and photodegradation method. *RSC Adv.* 2019; 9: 37686-95.
73. Fouda A, Saied E, Eid A. M, Kouadri F, Alemam A. M, Hamza M. F, Alharbi M, Elkelish A and Hassan S. E. Green synthesis of zinc oxide nanoparticles using an aqueous extract of *Punica granatum* for antimicrobial and catalytic activity. *Funct. Biomater* 2023; 14 :205.
74. Sharma A, Thakur M, Kumar A, Gautam M, Kumari S, Pathania D and Sharma A. Efficient photodegradation of fast sulphon black and crystal violet dyes from water systems using locust bean gum (LBG)-encapsulated zirconium-based nanoparticles and antibacterial activity. 2023; 8: 1-9.
75. Asgharian M, Mehdipourghazi M, Khoshandam B and Keramati N. Photocatalytic degradation of methylene blue with synthesized rGO/ZnO/Cu. *Chem. Phys. Lett.,* 2019; 719: 1-7.
76. Manea Y. K and Khan A. M. Enhanced photocatalytic degradation of methylene blue and adsorption of metal ions by SDS-TiP nanocomposite. *SN Appl. Sci*., 2019; 1: 1-5.
77. Pan G, Xu M, Zhou K, Meng Y, Chen H, Guo Y and Wu T. Photocatalytic degradation of methylene blue over layered double hydroxides using various divalent metal ions. *Clay Miner.,* 2019; 67: 340-7.
78. He Y, Jiang D. B, Chen J and Zhang Y. X. Synthesis of MnO2 nanosheets on

montmorillonite for oxidative degradation and adsorption of methylene blue. *J. Colloid Interface Sci.,* 2018; 510: 207-20.

79. Ai L and Li L. Efficient removal of organic dyes from aqueous solution with ecofriendly biomass-derived carbon@ montmorillonite nanocomposites by one-step hydrothermal process. *Chem. Eng. J.* 2013; 223: 688-95.
80. Chen C, Mi S, Lao D, Shi P, Tong Z, Li Z and Hu H. Single-step synthesis of eucalyptus sawdust magnetic activated carbon and its adsorption behavior for methylene blue. *RSC Adv.,* 2019; 9: 22248-62.
81. Fan L, Zhang Y, Luo C, Lu F, Qiu H and Sun M. Synthesis and characterization of magnetic β-cyclodextrin–chitosan nanoparticles as nano-adsorbents for removal of methyl blue. *Int. J. Biol. Macromol.,* 2012; 50: 444-50.
82. Priya J. R, Mercina M, Nancy MP, Linet J. M and Mani J. A. Synthesis and characterization of rhodamine b and methylene blue doped potassium hydrogen phthalate single crystals. *Mater. Today.*, 2022; 65: 385-90.
83. Foroutan R, Peighambardoust S. J, Peighambardoust S. H, Pateiro M and Lorenzo J. M. Adsorption of crystal violet dye using activated carbon of lemon wood and activated carbon/Fe3O4 magnetic nanocomposite from aqueous solutions: a kinetic, equilibrium and thermodynamic study. *Mol.*, 2021; 26.